

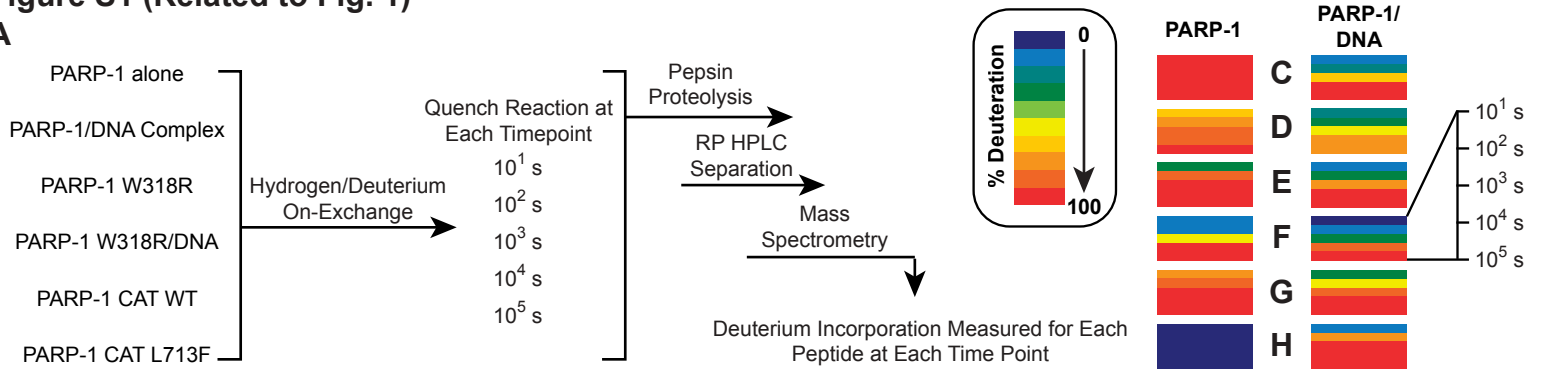
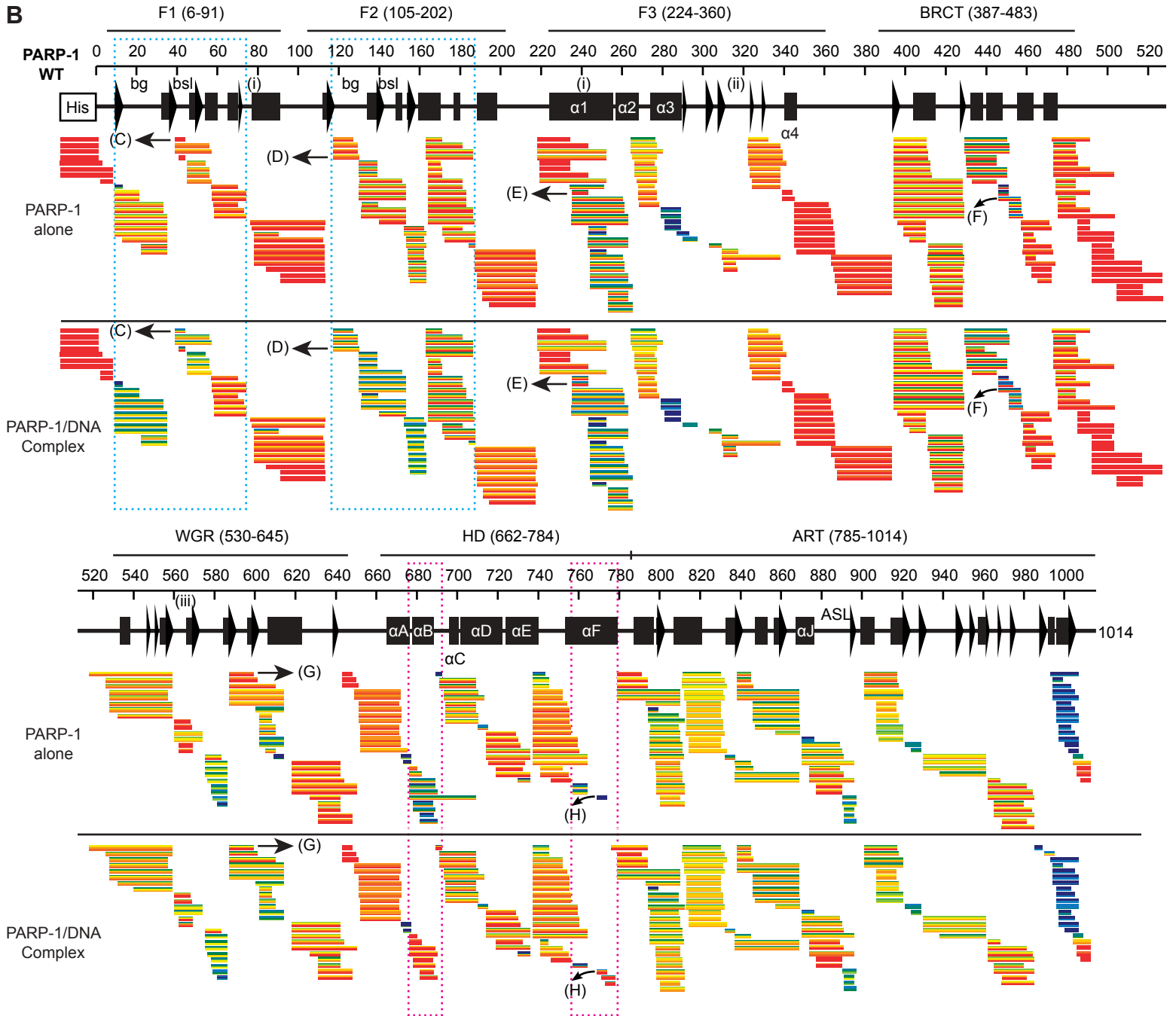
Figure S1 (Related to Fig. 1)**A****B**

Figure S1.

(A) Experimental scheme for HXMS. In HXMS, a protein is incubated with heavy water (D_2O), and the exchange of amide hydrogens for deuterium on the polypeptide backbone is detected as an increase in mass and is measured over a time course to provide the rates of HX. Amide protons are protected from HX when they participate in hydrogen bonds, for example within an α -helix or the interior of a β -sheet. Molecular contacts can stabilize secondary structural elements and thus further protect amide protons from HX. Thus, the rates of HX can also report on changes in protein structure and dynamics from one condition to another (e.g. PARP-1 bound to DNA damage *versus* PARP-1 alone), in addition to providing insights into the relative rates of exchange for different regions of a protein.

(B) HXMS data for PARP-1 alone and the PARP-1/DNA complex. Each horizontal bar represents an individual peptide, and the 5 stripes within each bar are colored according to percentage deuteration at each of the 5 time points (10^1 s, 10^2 s, 10^3 s, 10^4 s, 10^5 s). Boxes highlight regions with the greatest increased protection (cyan) from HX in the PARP-1/DNA complex compared to PARP-1 alone and with the greatest decreased protection (magenta). bg, backbone grip; bsl, base stacking loop; (i) F1-F3 interface; (ii) Z3/WGR/HD interface; (iii) WGR/HD interface. When available, we present the data for all measurable charge states of the 336 and 329 unique peptides for PARP-1 alone and PARP-1/DNA complex, respectively.

(C-H, top right) Peptides indicated with arrows in panel B are redisplayed for (left) PARP-1 alone and (right) the PARP-1/DNA complex.

Figure S2 (Related to Fig. 1)

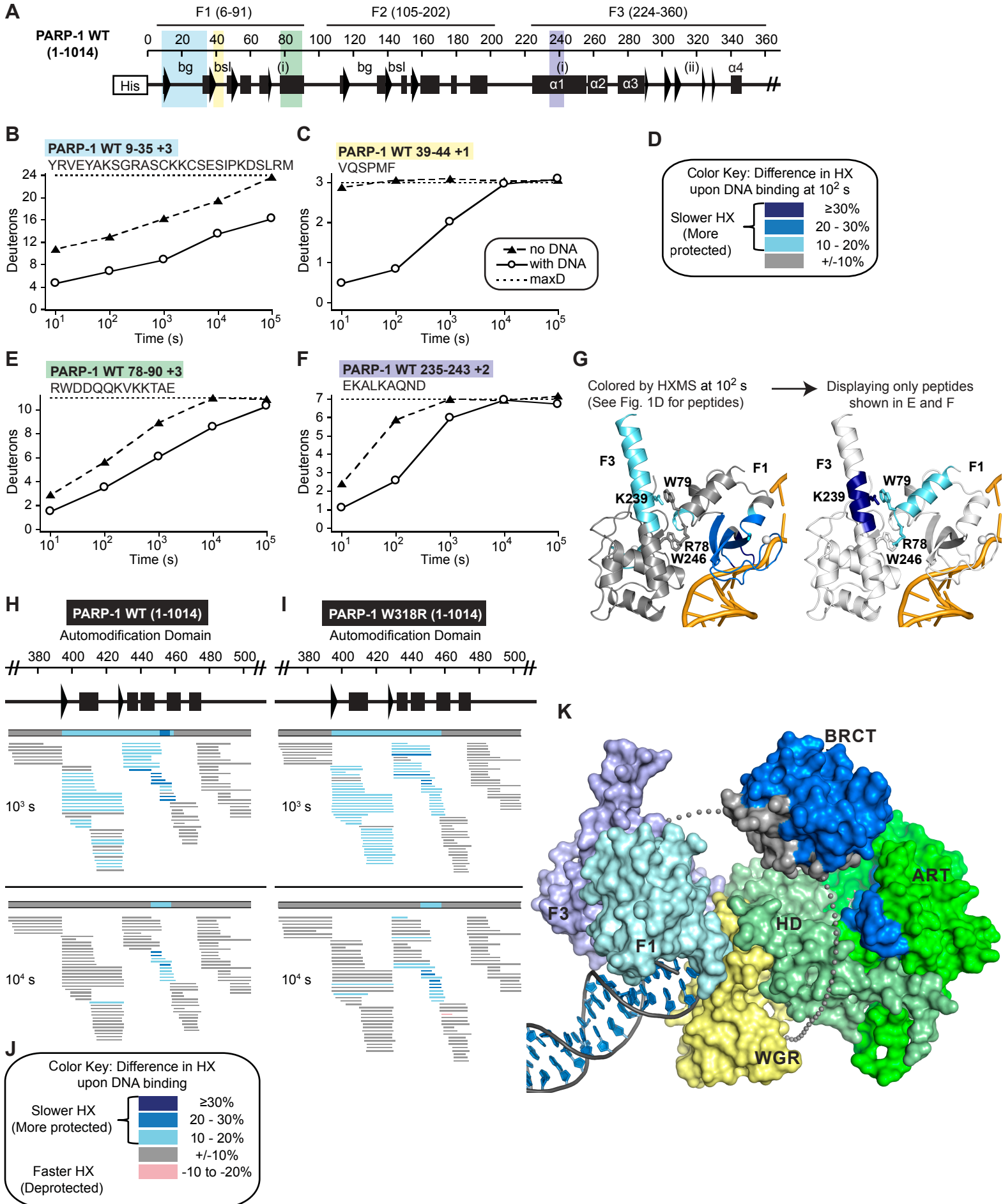


Figure S2.

(A) Schematic of PARP-1 highlighting peptides displayed in (B-C) and (E-F). bg, backbone grip; bsl, base stacking loop; (i) F1-F3 interface; (ii) Z3/WGR/HD interface.

(B-C) HXMS of peptides from the F1 DNA binding interface of PARP-1. The calculated maximum number of exchangeable deuterons (maxD) is indicated.

(D) Color key for the binning of HX differences. Percent difference is calculated by subtracting the percent deuteration of PARP-1 in complex with DNA from that of PARP-1 alone.

(E-F) HXMS of peptides from (E) F1 helix a.a. 78-91 and (F) F3 α 1-helix at the F1-F3 interface of PARP-1. The calculated maximum number of exchangeable deuterons (maxD) is indicated.

(G) HXMS data from Fig. 1D for PARP-1 at the 100 s time point is mapped onto the structure of the F1-F3 interface of the PARP-1/DNA complex and plotted using the color key in (D). Consensus HXMS data is used on the left while individual peptides from (E, F) are colored on the right.

(H-I) Percent difference in HX is calculated for each peptide (represented by horizontal bars) by subtracting the percent deuteration of PARP-1 in complex with DNA from that of PARP-1 alone at the 10^3 s and 10^4 s time points for (H) PARP-1 WT and (I) PARP-1 W318R and plotted using the color key in (J). The consensus behavior at each residue is displayed above the peptides at each time point. When available, we present the data for all measurable charge states of the 120 and 147 unique peptides for (H) and (I), respectively).

(J) Color key for the binning of HX differences. Percent difference is calculated by subtracting the percent deuteration of PARP-1 in complex with DNA from that of PARP-1 alone.

(K) Surface representation of PARP-1 essential domains based on the crystal structure (Langelier et al., 2012) with the same domain coloring shown in Fig. 1 A and 1B. The BRCT domain structure (PDB code 2cok) and linker residues connecting the F3 to BRCT, and BRCT to WGR have been manually modeled to illustrate how the conformation of PARP-1 bound to DNA damage positions the AD (automodification

domain, see Fig. 1A) in close proximity to the catalytic domain (Langelier and Pascal, 2013). HXMS analysis indicated that a region of the ART and portions of the BRCT (colored blue) showed increased HX protection when PARP-1 was bound to DNA damage (also see Fig. 1D and Fig. S2H) relative to that observed in the absence of DNA damage. We interpret these HXMS changes to reflect contacts formed between the AD and the CAT when PARP-1 is poised for automodification. Unlike most other regions of the PARP-1 polypeptide, the peptides detected for HXMS analysis of the AD did not allow us to more narrowly define the regions of increased protection.

Figure S3 (Related to Fig. 2)

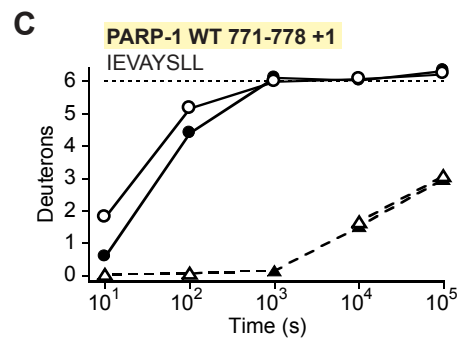
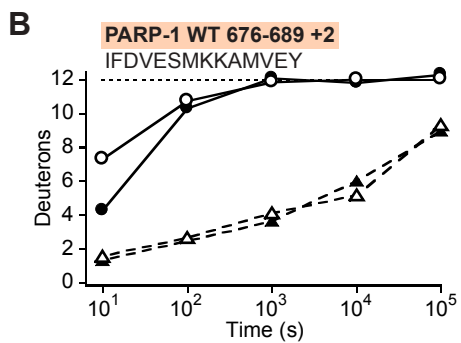
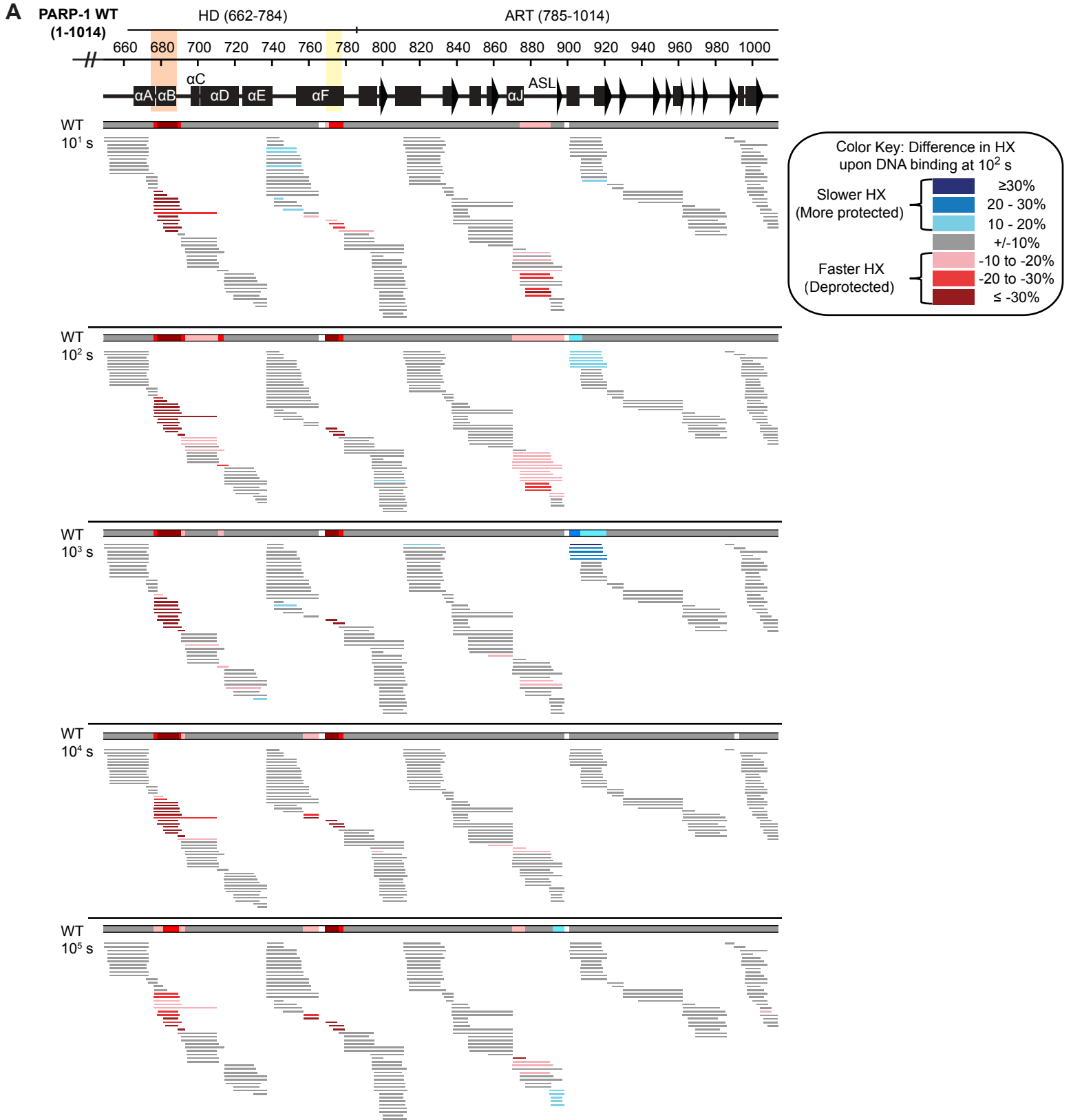
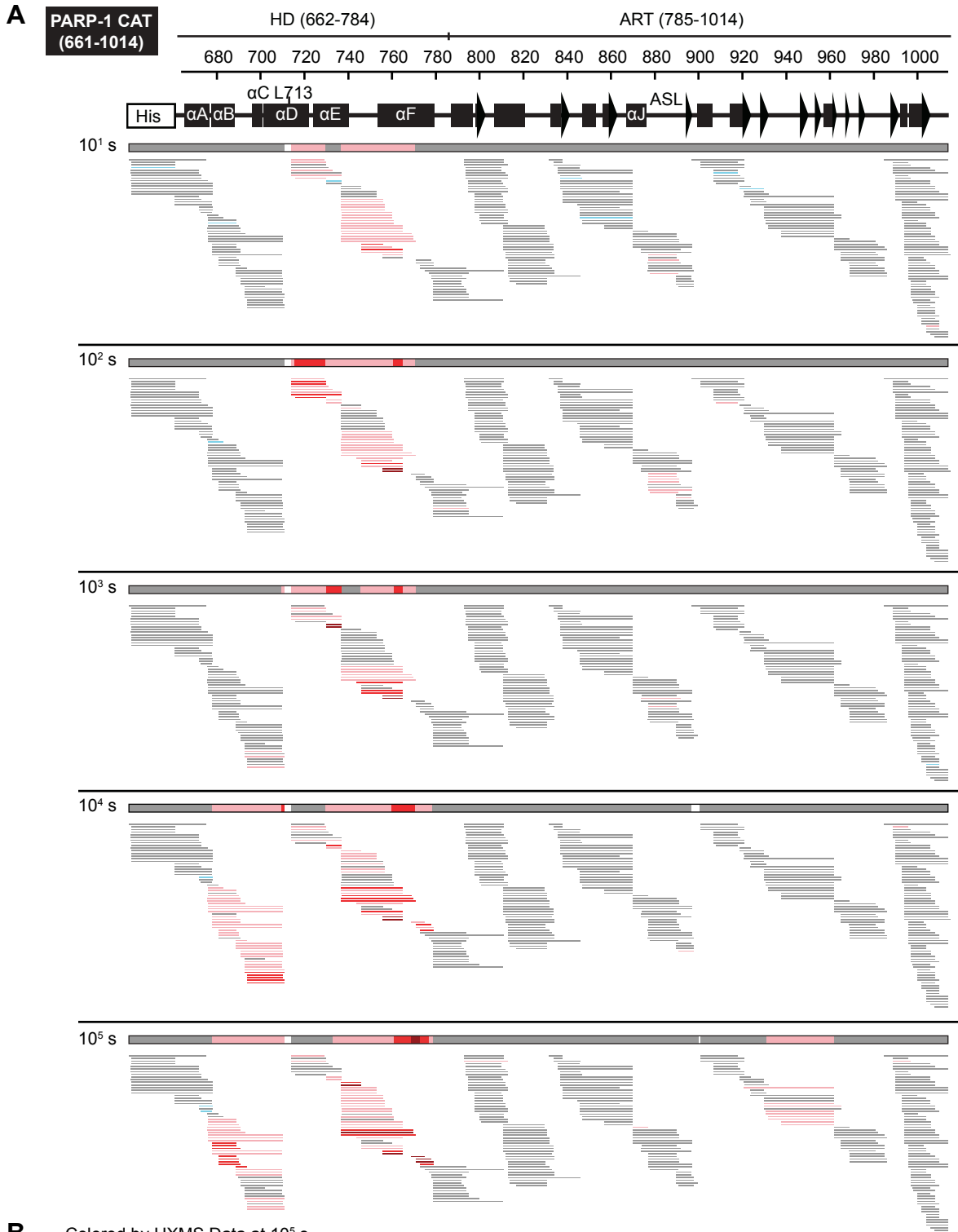


Figure S3.

(A) Percent difference in HX is calculated for each peptide (represented by horizontal bars) by subtracting the percentage deuteration of PARP-1 in complex with DNA from that of PARP-1 alone at the 10^1 s, 10^2 s, 10^3 s, 10^4 s, and 10^5 s time points. Only CAT domain peptides are shown. The consensus behavior at each residue is displayed above the peptides at each time point. White indicates a gap in peptide coverage. When available, we present the data for all measurable charge states of the 143, 146, 136, 145, and 139 unique peptides at the 10^1 s, 10^2 s, 10^3 s, 10^4 s, and 10^5 s time points, respectively.

(B-C) HXMS of representative peptides from the α B in (B), and the C-terminal end of α F in (C) for PARP-1 alone and PARP-1 in complex with DNA from 2 independent on-exchange reactions. The calculated maximum number of exchangeable deuterons (maxD) is indicated.

Figure S4 (Related to Fig. 2)



B Colored by HXMS Data at 10^5 s

PARP-1 CAT

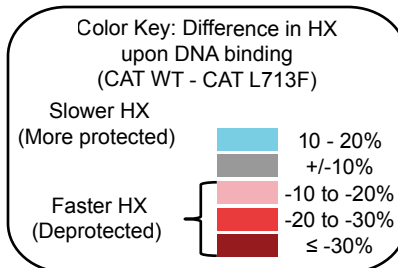
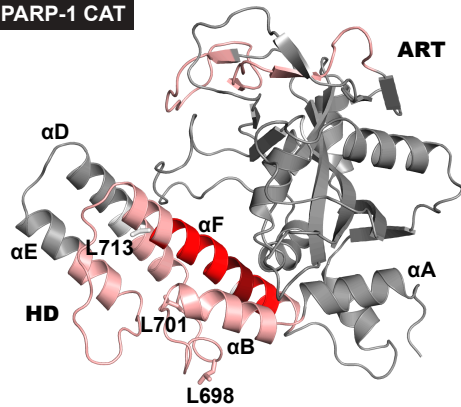


Figure S4.

(A) Percent difference in HX is calculated for each peptide (represented by horizontal bars) by subtracting the percent deuteration of PARP-1 CAT L713F from that of PARP-1 CAT at the 10^1 s, 10^2 s, 10^3 s, 10^4 s, and 10^5 s time points. The consensus behavior at each residue is displayed above the peptides at each time point. White indicates a gap in peptide coverage. When available, we present the data for all measurable charge states of the 201, 205, 203, 208, and 204 unique peptides at the 10^1 s, 10^2 s, 10^3 s, 10^4 s, and 10^5 s time points, respectively.

(B) Consensus HXMS data from (A, 10^5 s) is mapped onto the structure of the catalytic domain of the PARP-1/DNA complex.

Figure S5 (Related to Fig. 3)

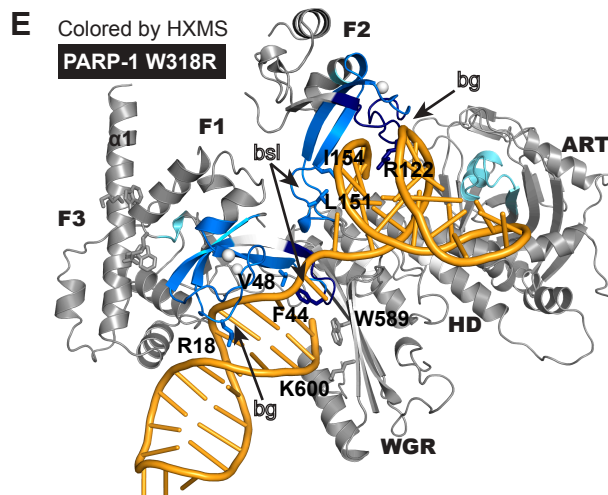
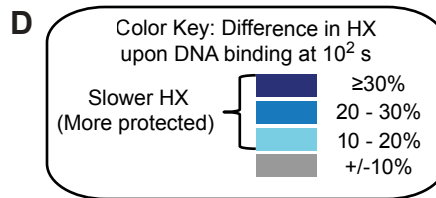
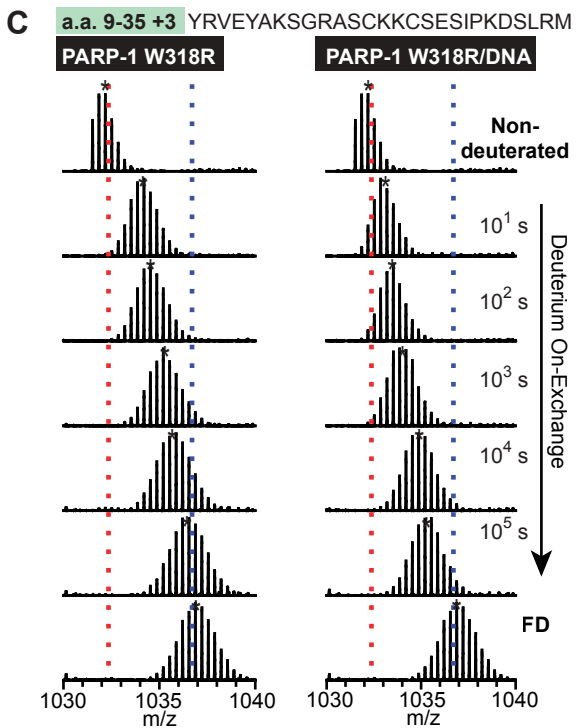
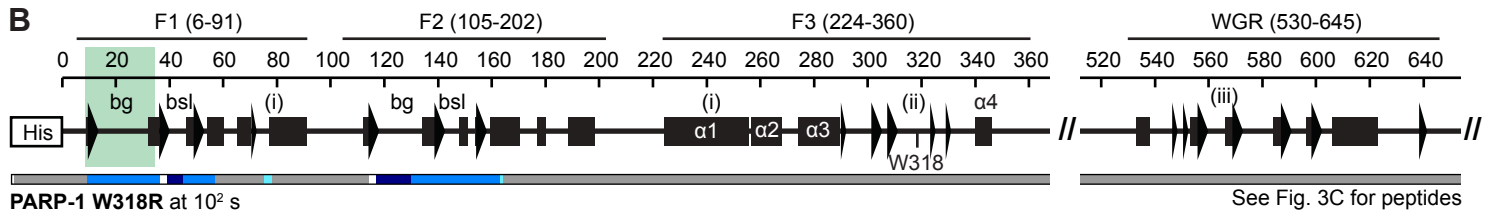
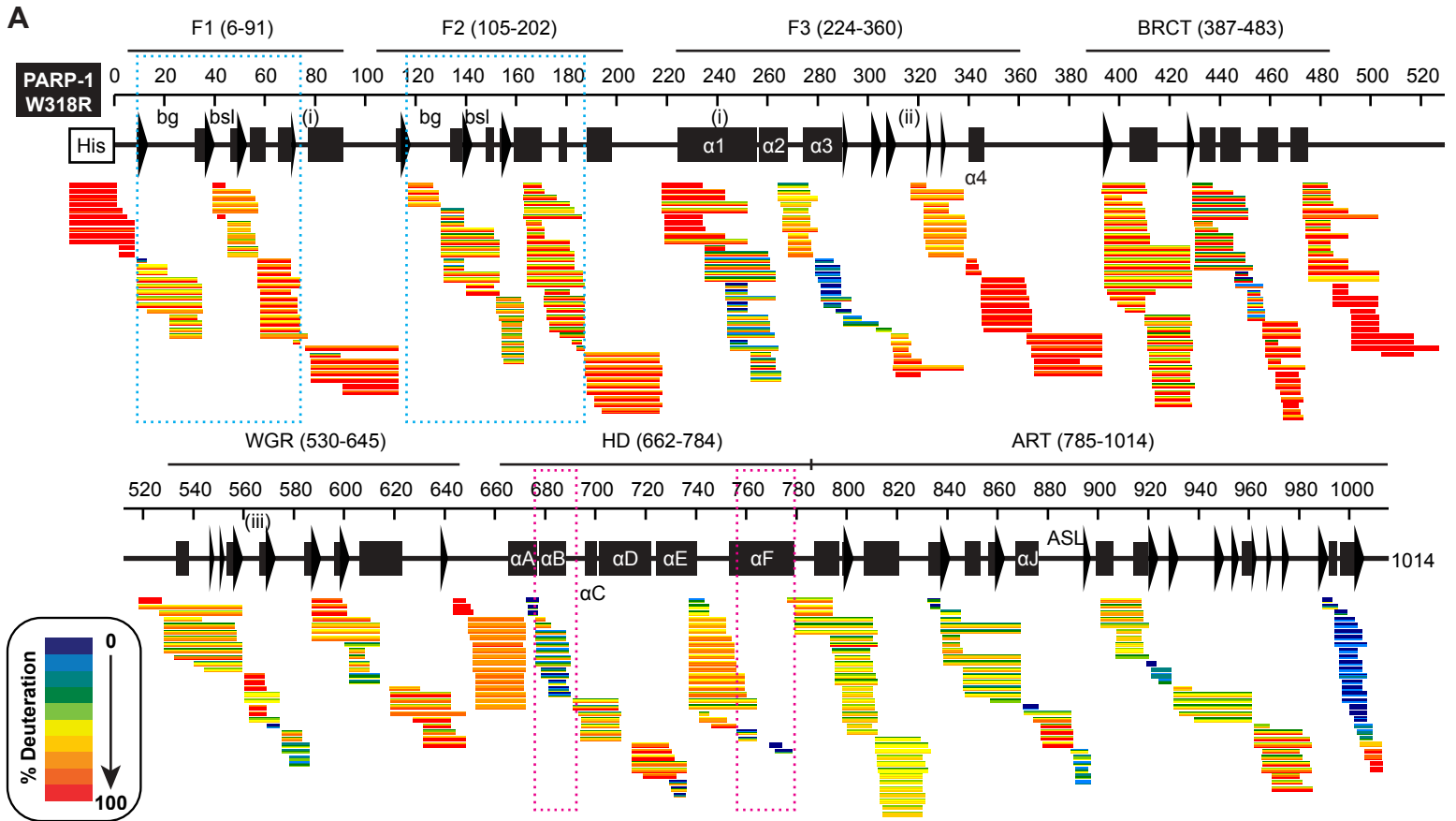


Figure S5.

(A) HXMS data for PARP-1 W318R alone. Each horizontal bar represents an individual peptide, and the 5 stripes within each bar are colored according to percentage deuteration at each of the 5 time points (10^1 s, 10^2 s, 10^3 s, 10^4 s, 10^5 s). Cyan and magenta boxes are identical to those in Fig. S1B and are shown for comparison. bg, backbone grip; bsl, base stacking loop; (i) F1-F3 interface; (ii) Z3/WGR/HD interface; (iii) WGR/HD interface. When available, we present the data for all measurable charge states of the 383 unique peptides.

(B) Consensus percent difference in HX for PARP-1 W318R at the 100 s time point from Fig. 3C is redisplayed. See color key in (D).

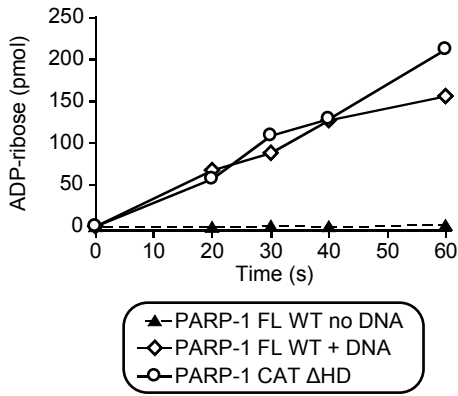
(C) Raw MS data from peptide highlighted in green in (B). Centroid values are indicated (*). Red and blue dotted lines are drawn as guides for visualizing differences. FD is the fully deuterated condition used for normalization due to back-exchange.

(D) Color key for the binning of HX differences. Percent difference is calculated by subtracting the percent deuteration of PARP-1 W318R in complex with DNA from that of PARP-1 W318R alone.

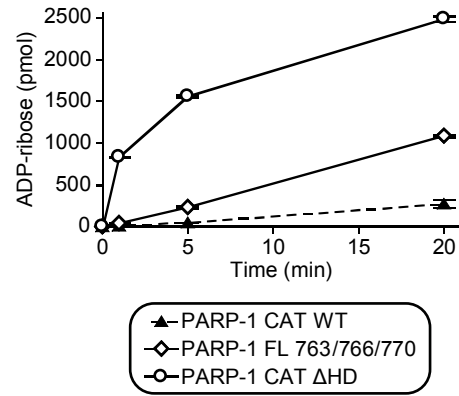
(E) Consensus percent difference in HX for PARP-1 W318R at the 100s time point (B) is mapped onto the structure of the DNA binding interface and plotted using the color key in (D).

Figure S6 (Related to Figs. 4-6)

A



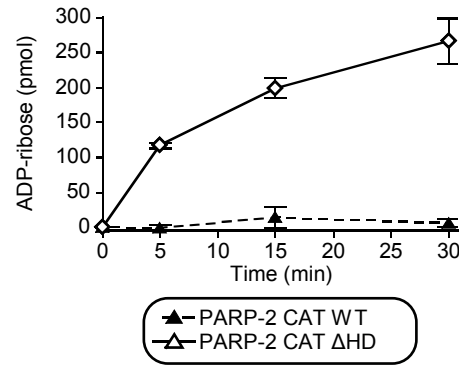
E



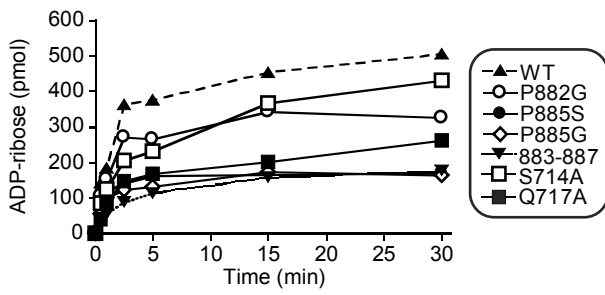
B

Construct	Initial rate (pmol/s) Avg ± stdev
PARP-1 FL WT + DNA	4.1 ± 2.6
PARP-1 CAT ΔHD	5.2 ± 2.4

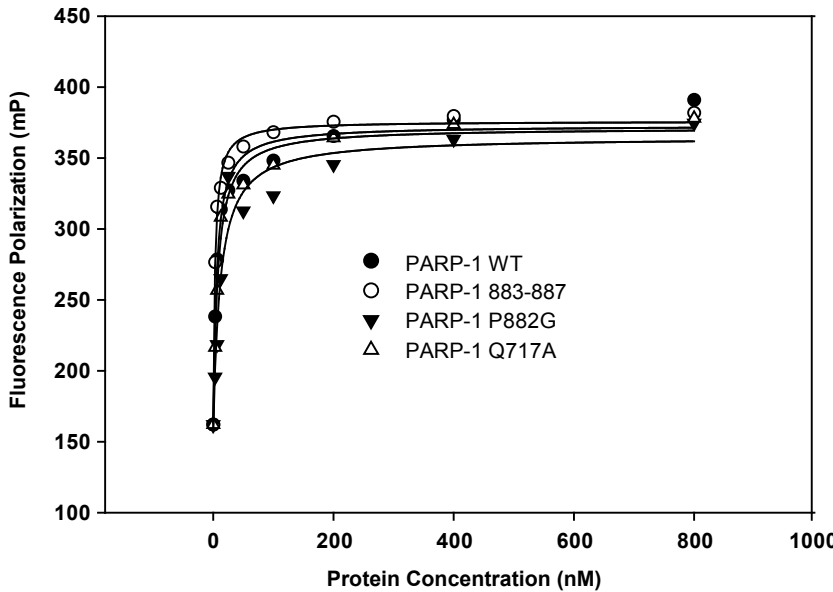
F



C



D



PARP-1 WT	a0= 164.2+/-11.8 a1= 372.9+/-6.2 Kd= 5.8+/-1.2
PARP-1 883-887	a0= 162.9+/-6.2 a1= 375.9+/-3.2 Kd= 2.9+/-0.3
PARP-1 P882G	a0= 156.5+/-17.0 a1= 364.7+/-11.1 Kd= 11.4+/-3.8
PARP-1 Q717A	a0= 160.3+/-9.6 a1= 371.2+/-5.3 Kd= 7.3+/-1.2

Figure S6.

(A) Representative colorimetric assay data comparing the activity of the PARP-1 CAT Δ HD to that of PARP-1 FL WT in the presence or absence of DNA. Protein (20 nM) and DNA (40 nM) were incubated with 500 mM NAD^+ ($\text{NAD}^+:\text{bio-NAD}^+$, 99:1) for the indicated time points in the linear range of product formation.

(B) The initial rate of product formation was calculated from slope of the data in panel (A). The averages and standard deviations of three independent experiments are shown.

(C) DNA-dependent activity of PARP-1 helix D/ASL mutants. Colorimetric assay showing the DNA-dependent activity of PARP-1 WT and mutants. Protein (20 nM) and DNA (40 nM) were incubated with 500 mM NAD^+ ($\text{NAD}^+:\text{bio-NAD}^+$, 99:1) for various time points.

(D) PARP-1 ASL and helix D mutants are not deficient in DNA binding. The binding affinities of PARP-1 WT and mutants were determined by Fluorescence Polarization. The values shown are the binding constants calculated by fitting the data to a two-state binding model.

(E-F) Colorimetric assay showing the activity of (E) PARP-1 CAT Δ HD, PARP-1 CAT WT, and PARP-1 FL D763A/E766A/E770A triple mutant and (F) PARP-2 CAT Δ HD and PARP-2 CAT WT. Proteins (60 nM in panel E, 20 nM in panel F) were incubated with 500 μM NAD^+ ($\text{NAD}^+:\text{bio-NAD}^+$, 99:1) for the indicated time points. Experiments were performed in triplicate with the average values plotted and the error bars representing the standard deviations.

SUPPLEMENTAL EXPERIMENTAL PROCEDURES

Gene cloning and Mutagenesis The PARP-1 CAT Δ HD construct used for crystallization was created by replacing PARP-1 residues 678–787 with an 8-residue linker (GSGSGSGG) in a pET28 construct coding for PARP-1 residues 661–1011. The PARP-2 CAT Δ HD construct used for crystallization was created by deleting residues 241–334 from a pET28 construct coding for PARP-2 isoform 2 residues 216–570. The PARP-2 FL Δ HD construct was created by deleting PARP-2 residues 260–334 from a pET28 PARP-2 isoform 2 FL construct (residues 1 to 570). The PARP-3 FL Δ HD construct was created by deleting PARP-3 residues 205–299 from a pDEST17 PARP-3 isoform b FL construct (residues 1 to 533; a gift from Dr. Ivan Ahel). Deletion of the HD in full-length PARP-1 was initially not possible due to toxicity issues apparent at mutagenesis steps and when using cloning strains of *E. coli* that are not engineered to specifically produce heterologous proteins. We overcame this limitation by preparing full-length PARP-1 using sortase-mediated joining of two PARP-1 fragments (N-terminal fragment and C-terminal fragment). The C-terminal fragment, which contains the catalytic domain bearing the HD deletion, still exhibited toxicity during cloning and expression; however, this level of toxicity could be mitigated through the use of a PARP inhibitor during cloning and protein production. Sortase fragment 1 was produced from a pET24 construct coding for residues 1–375 and a C-terminal linker LPTEG (sortase recognition sequence). Sortase fragment 2 was produced from a pET28 construct coding for residues 383–703/779–1014 with an N-terminal sumo tag (SMT) that was removed during purification. PARP-1 site-directed mutagenesis was performed using pET28 PARP-1 FL (residues 1 to 1014) using the QuikChange protocol (Stratagene). Sequences were verified by automated sequencing (Sidney Kimmel Cancer Center).

Protein Purification PARP-1 FL WT and mutants were expressed and purified as described previously using three chromatography steps (Ni²⁺ affinity, heparin-sepharose, and gel filtration) (Langelier et al., 2011b; Langelier et al., 2008). PARP-1 CAT WT, CAT L713F, CAT Δ HD were expressed and purified as described for PARP-1 CAT WT (Langelier et al., 2012). PARP-2 FL WT, PARP-2 FL Δ HD, PARP-3 FL and PARP-3 FL Δ HD were purified as described (Langelier et al., 2014). PARP-2 CAT WT and CAT

Δ HD were purified as described (Langelier et al., 2014) with the exception that the flow through from the Ni^{2+} affinity column was diluted to a final concentration of 50 mM NaCl in the heparin column buffer. The PARP-1 FL Δ HD protein was produced by sortase-mediated joining of two PARP-1 fragments. The pET24 1–375 LPTEG fragment was purified as described (Langelier et al., 2011b; Langelier et al., 2008). The pET28 SMT–PARP-1 383–703/779–1014 fragment was purified as described (Langelier et al., 2008) with the following modifications. The protein was eluted from a Ni^{2+} column with 400 mM imidazole and treated with the ULP1 protease (1 hour at 4°C) to remove the SMT tag and create an N-terminal GGG sequence for the sortase reaction. The mixture was then diluted to lower the imidazole concentration to 40 mM and passed over a Ni^{2+} column to remove the SMT tag. The Ni^{2+} -column flow-through was further diluted to lower the NaCl concentration to 250 mM NaCl prior to loading onto a heparin column, which was then eluted as described (Langelier et al., 2008). The sortase reaction was performed based on the following study (Huang et al., 2003) using 245 μM of 383–1014, 510 μM 1–375 LPETG, and 5.4 μM sortase in a 500 μL reaction in sortase buffer (50 mM Tris pH 8.0, 50 μM ZnSO_4 , 1 mM DTT, 10 mM CaCl_2 , 200 mM NaCl). The sortase reaction was dialyzed at 4°C overnight, and then passed over a Ni^{2+} column. The sortase reaction removed the His-tag from 1-375 LPETG, thus the FL Δ HD protein was found in the flow-through of the Ni^{2+} column, which was then diluted to bring the NaCl concentration to 250 mM for loading onto a heparin column. The heparin column was then eluted as described and the fractions containing the PARP-1 FL Δ HD protein were pooled, dialyzed (25 mM Hepes pH 8.0, 150 mM NaCl, 1 mM EDTA, 0.1 mM TCEP) and concentrated. Note that the PARP-1 FL Δ HD produced using this method has an internal deletion between residues 375 and 383 and a linker addition (LPETGGG) that restores PARP-1 to the same total number of amino acid residues. The purified Sortase from *S. Aureus* was a kind gift from S. Eustermann and D. Neuhaus. For overactive PARP-1, PARP-2 and PARP-3 mutants, 10 mM benzamide was added to the *E.coli* media to reduce cellular toxicity of the PARP protein.

Complex preparation for HXMS PARP-1 was assembled onto DNA damage prior to HXMS analysis. To model DNA damage, we used a dumbbell DNA in which each end of a DNA duplex contains hairpin turns and one strand has a centrally placed gap representing a single-strand break (Eustermann et al.,

2015). The DNA (deoxy nucleotide sequence:

GCTGGCTTCGTAAGAAGCCAGCTCGCGGTCAGCTTGCTGACCGCG) was annealed in pre-HXMS buffer (10 mM HEPES, pH 7.0, 150 mM NaCl, 1 mM EDTA, and 0.1 mM TCEP). All PARP-1 constructs were dialyzed into pre-HXMS buffer. PARP-1/DNA complexes were assembled at room temperature for 30 minutes by incubating PARP-1 (~1 µg/µL) with the 45-nucleotide DNA at a molar ratio of 1:1.2 (protein:DNA) in pre-HXMS buffer.

HX reactions Deuterium on-exchange was performed at room temperature (RT) by adding 5 µL of each sample (~14 µg of CAT truncation constructs, ~5 µg of full-length PARP-1 constructs) to 15 µL of deuterium on-exchange buffer (10 mM HEPES, pH 7.0, 150 mM NaCl) for a final D₂O content of 75%. A 20 µL aliquot was removed at each time point, and the reaction was quenched with 30 µL ice-cold quench buffer (1.66 M guanidine hydrochloride, 10% glycerol, and 0.8% formic acid, for a final pH of 2.4–2.5) and rapidly frozen in liquid nitrogen. The samples were stored at -80°C prior to analysis by MS.

Protein fragmentation and MS Each HX sample (50 µL) was thawed on ice and injected into an on-line temperature-controlled system, as previously described (DeNizio et al., 2014). Samples were first pumped over an immobilized pepsin column. Pepsin (Sigma) was coupled to POROS 20 AL support (Applied Biosystems), and the immobilized pepsin was packed into a column housing (2 mm x 2 cm, Upchurch). Peptides were collected onto a C18 trap column (800 µm x 2 mm, Dionex). Once denaturant and salts were washed away, peptides were eluted onto and separated by an HPLC C18 analytical column (0.3 mm x 75 mm, Agilent). PARP-1 CAT constructs were eluted by a linear 18-45 % buffer B gradient (Buffer A: 0.1% formic acid; Buffer B: 0.1% formic acid, 99.9% acetonitrile) over 15 min at 6 µL/min. For full-length PARP-1, a shaped chromatographic gradient was used so that the number of peptides eluted per unit time was roughly uniform over the 20 min gradient. The effluent was electrosprayed into the mass spectrometer (LTQ Orbitrap XL, Thermo Fisher Scientific). Non-deuterated (ND) samples were prepared in ND exchange buffer (10 mM HEPES, pH 7.0, 150 mM NaCl) in the absence of D₂O and each 20 µL aliquot was ‘quenched’ with 30 µL ice-cold quench buffer.

Peptide identification We analyzed MS/MS data collected from ND samples to identify potential PARP-1 peptides using SEQUEST (Bioworks v3.3.1, Thermo Fisher Scientific) with a peptide tolerance of 8 ppm and a fragment tolerance of 0.1 AMU. We discarded peptides that failed to meet a specified quality score (SEQUEST P_{pep} score < 0.99) or whose sequence could be found at more than one place in the protein. Non-deuterated and deuterated peptides were identified and their centroid masses were determined using the ExMS data analysis program as is described in detail elsewhere (Kan et al., 2011). Briefly, peptides were identified in MS scans based upon a number of spectral and chromatographic properties: monoisotopic mass, charge state, isotopic peak positions and their distribution, maximum number of exchangeable and measurable deuterons (maxD, i.e. the number of amino acid residues excluding proline minus 2, see Kan et al., 2011), and retention time of the peptide in MS/MS scans. The $\Delta m/z$ tolerance was set at 10 ppm and 20 ppm for non-deuterated and deuterated peptides, respectively. Isobaric peptides that could not be discriminated were excluded from analysis.

HXMS measurement and analysis The level of HX reported for each peptide at each time point takes into account corrections for deuterium loss by individual peptides after quenching and during HXMS data collection (i.e. back-exchange). To correct for back-exchange, deuterated peptides are normalized to peptides from a 'fully-deuterated' (FD) reference sample, as described previously (DeNizio et al., 2014). Reference samples were deuterated under denaturing conditions (final 0.375% formic acid and D_2O content of 75%) for 2 days at RT, and a 20 μL aliquot was quenched with 30 μL ice-cold FD quench buffer (1.66 M guanidine hydrochloride, 10% glycerol, and 0.5% formic acid, for a final pH of 2.4 - 2.5) and rapidly frozen in liquid nitrogen. To be included in analysis, therefore, each individual deuterated peptide must have also been found in the non-deuterated and fully deuterated states (identical residues and charge state).

HXMS plotting Peptide plotting and calculations were performed in MATLAB. Plots reporting percent deuteration (Fig. S1B; Fig. S5A) include all peptides for which the identical peptide was found across all five time points, the ND, and FD samples for a given condition. Plots reporting percent difference in HX include all peptides for which the identical peptide was found in both conditions (e.g. alone and in

complex with DNA), the ND, and FD samples. Consensus behavior at each residue was calculated as the average of the differences in HX protection of all peptides spanning that residue (Fig. 1D; Fig. 3C; Fig. S2H-I; Fig. S3A; Fig. S4A). We include in our figures peptides of identical sequence but different charge states. Although not unique peptides, they do add confidence to our peptide identification since their deuteration levels are in close agreement with each other. The HXMS peptides plotted that span the length of PARP-1 all come from one experiment collected within a 24 h window in order to avoid slight changes in fragmentation patterns between independently performed experiments that were collected at different points in time. This choice in presentation allows us to maximize the number of peptides (identified by both a given sequence and charge state) that we can identify in both the non-deuterated and fully deuterated samples as well as between conditions across time points. Nonetheless, the findings reported in this paper regarding the dynamics of each of the domains of PARP-1 are representative of the results of multiple experiments.

SDS-PAGE assay The SDS-PAGE assay was performed as described previously (Langelier et al., 2008) using 1 μ M protein, 1 μ M DNA and 0.5 mM NAD^+ where indicated.

Colorimetric Assay The colorimetric assays were performed essentially as described for PARP-1, PARP-2, and PARP-3 (Langelier et al., 2014; Langelier et al., 2008). In Fig. 5, Fig. 7 and Fig. S6E, 60 nM of PARP-1 WT or mutant was incubated for the indicated time points with a mixture of NAD^+ and biotinylated NAD^+ (bio- NAD^+) at a 99:1 ratio (500 μ M total concentration). In Fig. S6A-B, 20 nM of protein and 40 nM DNA were used. The colorimetric assay for PARP-2 WT and PARP-2 Δ HD (Fig. 4B; Fig. S6F) was performed using 20 nM protein and 500 μ M NAD^+ (NAD^+ :bio- NAD^+ , 99:1). For PARP-3 WT and PARP-3 Δ HD (Fig. 4C), 60 nM protein was incubated with 25 μ M NAD^+ (NAD^+ :bio- NAD^+ , 4:1).

Crystallization and Structure Determination PARP-1 CAT Δ HD (30 mg/mL) was crystallized with olaparib (1 mM in DMSO, 10% final) in 20-25% PEG 3350, 0.2 M Ammonium Sulfate, 0.1 M Bis-Tris pH 5.5 in sitting drop trays at room temperature. Crystals were flash-cooled in liquid nitrogen directly after transfer from the growth drop. PARP-2 CAT Δ HD (25 mg/mL) was crystallized with EB-47 (850

μM) in 2.55-2.65 M NaCl and 0.1 M Tris pH 7.5-8.5. Crystals were cryo-protected in 2.6 M NaCl, 0.1 M Tris pH 8.0, and 20% glycerol prior to flash-cooling in liquid nitrogen. X-ray diffraction data were collected at SIBYLS beamline 12.3.1 (Advance Light Source) and processed using XDS (Kabsch, 2010) (Table 1). The structures were determined by molecular replacement using PHASER (McCoy, 2007) as implemented in the PHENIX suite (Adams et al., 2010). PDB code 3gjl (Karlberg, et al., 2010) with the HD removed was the search model for PARP-1 CAT Δ HD, and PDB code 3kjd (Miyashiro et al., 2009) with the HD removed was the search model for PARP-2 CAT Δ HD. Model building was performed using COOT (Emsley et al., 2010) and refinement was performed using PHENIX (Adams et al., 2010), REFMAC5 (Murshudov et al., 2011; Winn et al., 2011), and PDB_REDO (Joosten et al., 2014). Structure images were made using PYMOL Molecular Graphics System (Schrödinger, LLC).

SUPPLEMENTAL REFERENCES

- Adams, P.D., Afonine, P.V., Bunkoczi, G., Chen, V.B., Davis, I.W., Echols, N., Headd, J.J., Hung, L.W., Kapral, G.J., Grosse-Kunstleve, R.W., *et al.* (2010). PHENIX: a comprehensive Python-based system for macromolecular structure solution. *Acta Crystallogr D Biol Crystallogr* *66*, 213-221.
- DeNizio, J.E., Elsasser, S.J., and Black, B.E. (2014). DAXX co-folds with H3.3/H4 using high local stability conferred by the H3.3 variant recognition residues. *Nucleic Acids Res* *42*, 4318-4331.
- Emsley, P., Lohkamp, B., Scott, W.G., Cowtan, K. (2010) Features and development of Coot. *Acta Crystallogr D Biol Crystallogr.* *66*, 486-501.
- Eustermann, S., Wu, W.-F., Langelier, M.-F., Yang, J.-C., Easton, L.E., Riccio, A.A., Pascal, J.M., and Neuhaus, D. (2015) Structural basis for DNA single-strand break detection and signaling by human PARP-1. *Mol Cell*.
- Huang, X., Aulabaugh, A., Ding, W., Kapoor, B., Alksne, L., Tabei, K., and Ellestad, G. (2003). Kinetic mechanism of *Staphylococcus aureus* sortase SrtA. *Biochemistry* *42*, 11307-11315.
- Joosten, R.P., Long, F., Murshudov, G.N., Perrakis, A. (2014) The PDB_REDO server for macromolecular structure model optimization. *IUCrJ* *1*, 213-20.
- Kabsch, W. (2010). Xds. *Acta Crystallogr D Biol Crystallogr* *66*, 125-132.
- Kan, Z.Y., Mayne, L., Chetty, P.S., and Englander, S.W. (2011). ExMS: data analysis for HX-MS experiments. *J Am Soc Mass Spectrom* *22*, 1906-1915.
- Karlberg, T., Hammarström, M., Schütz, P., Svensson, L., Schüler, H. (2010) Crystal structure of the catalytic domain of human PARP2 in complex with PARP inhibitor ABT-888. *Biochemistry* *49*, 1056-8.
- Langelier, M.F., Servent, K.M., Rogers, E.E., and Pascal, J.M. (2008). A Third Zinc-binding Domain of Human Poly(ADP-ribose) Polymerase-1 Coordinates DNA-dependent Enzyme Activation. *J Biol Chem* *283*, 4105-4114.
- Langelier, M.F., Planck, J.L., Roy, S., and Pascal, J.M. (2012). Structural basis for DNA damage-dependent poly(ADP-ribosyl)ation by human PARP-1. *Science* *336*, 728-732.
- Langelier, M.F., Planck, J.L., Servent, K.M., and Pascal, J.M. (2011b). Purification of human PARP-1 and PARP-1 domains from *Escherichia coli* for structural and biochemical analysis. *Methods Mol Biol* *780*, 209-226.
- Langelier, M.F., Riccio, A.A., and Pascal, J.M. (2014). PARP-2 and PARP-3 are selectively activated by 5' phosphorylated DNA breaks through an allosteric regulatory mechanism shared with PARP-1. *Nucleic Acids Res* *42*, 7762-7775.
- McCoy, A.J. (2007). Solving structures of protein complexes by molecular replacement with Phaser. *Acta Crystallogr D Biol Crystallogr* *63*, 32-41.

Miyashiro, J., Woods, K.W., Park, C.H., Liu, X., Shi, Y., Johnson, E.F., Bouska, J.J., Olson, A.M., Luo, Y., Fry, E.H., Giranda, V.L., Penning, T.D. (2009) Synthesis and SAR of novel tricyclic quinoxalinone inhibitors of poly(ADP-ribose)polymerase-1 (PARP-1). *Bioorg Med Chem Lett* *19*, 4050-4.

Murshudov, G.N., Skubák, P., Lebedev, A.A., Pannu, N.S., Steiner, R.A., Nicholls, R.A., Winn, M.D., Long, F., Vagin, A.A. (2011) REFMAC5 for the refinement of macromolecular crystal structures. *Acta Crystallogr D Biol Crystallogr* *67*, 355-67.

Winn, M.D., Ballard, C.C., Cowtan, K.D., Dodson, E.J., Emsley, P., Evans, P.R., Keegan, R.M., Krissinel, E.B., Leslie, A.G., McCoy, A., *et al.* (2011) Overview of the CCP4 suite and current developments. *Acta Crystallogr D Biol Crystallogr* *67*, 235-42.